



Transit time corrected arterial spin labeling technique aids to overcome delayed transit time effect

Tae Jin Yun^{1,2} · Chul-Ho Sohn^{1,2} · Roh-Eul Yoo^{1,2} · Kyung Mi Kang^{1,2} · Seung Hong Choi^{1,2} · Ji-hoon Kim^{1,2} · Sun-Won Park^{1,3} · Moonjung Hwang⁴ · R. Marc Lebel⁵

Received: 29 September 2017 / Accepted: 18 December 2017 / Published online: 29 December 2017
© Springer-Verlag GmbH Germany, part of Springer Nature 2017

Abstract

Purpose This study aimed to evaluate the usefulness of transit time corrected cerebral blood flow (CBF) maps based on multi-phase arterial spin labeling MR perfusion imaging (ASL-MRP).

Methods The Institutional Review Board of our hospital approved this retrospective study. Written informed consent was waived. Conventional and multi-phase ASL-MRPs and dynamic susceptibility contrast MR perfusion imaging (DSC-MRP) were acquired for 108 consecutive patients. Vascular territory-based volumes of interest were applied to CBF and time to peak (TTP) maps obtained from DSC-MRP and CBF maps obtained from conventional and multi-phase ASL-MRPs. The concordances between normalized CBF (nCBF) from DSC-MRP and nCBF from conventional and transition time corrected CBF maps from multi-phase ASL-MRP were evaluated using Bland-Altman analysis. In addition, the dependence of difference between nCBF (Δ nCBF) values obtained from DSC-MRP and conventional ASL-MRP (or multi-phase ASL-MRP) on TTP obtained from DSC-MRP was also analyzed using regression analysis.

Results The values of nCBFs from conventional and multi-phase ASL-MRPs had lower values than nCBF based on DSC-MRP (mean differences, 0.08 and 0.07, respectively). The values of Δ nCBF were dependent on TTP values from conventional ASL-MRP technique ($F = 5.5679$, $P = 0.0384$). No dependency of Δ nCBF on TTP values from multi-phase ASL-MRP technique was revealed ($F = 0.1433$, $P > 0.05$).

Conclusion The use of transit time corrected CBF maps based on multi-phase ASL-MRP technique can overcome the effect of delayed transit time on perfusion maps based on conventional ASL-MRP.

Keywords Cerebral blood flow · Cerebral hemodynamics · Arterial spin labeling · Perfusion-weighted MRI

Introduction

Due to technical advances in higher magnetic fields with efficient spin labeling, arterial spin labeling MR perfusion

imaging (ASL-MRP) has been incorporated as part of sequences in acquisition of MR imaging which is increasingly used in many neuroimaging applications, including acute and chronic cerebrovascular diseases, neoplasms, epilepsy, and functional MR [1–8]. In ASL-MRP, protons of arterial water in the feeding vasculature of the brain are magnetically labeled. These labeled arterial protons can flow through the vascular tree and exchange with proton in unlabeled brain tissue. Perfusion-weighted images can be generated by subtracting an image with inflowing labeled arterial spin from another image without such spin labeling [1, 9]. Compared to conventional dynamic susceptibility contrast MR perfusion imaging (DSC-MRP) or nuclear medicine imaging including PET or SPECT, ASL-MRP for perfusion measurement has the following main advantages: (1) it is completely non-invasive and (2) it provides absolute cerebral blood flow (CBF) information at brain tissue

✉ Chul-Ho Sohn
neurorad63@gmail.com

¹ Institute of Radiation Medicine, Seoul National University Medical Research Center, Seoul, Republic of Korea

² Department of Radiology, Seoul National University Hospital, 101, Daehangno, Jongno-gu, Seoul 03080, Republic of Korea

³ Department of Radiology, Seoul National University Boramae Medical Center, Seoul, Republic of Korea

⁴ GE Healthcare Korea, Seoul, Republic of Korea

⁵ GE Healthcare Canada, Calgary, Canada

level without exposing patient to radiation or contrast media.

However, many factors can generate errors in quantitative estimation of CBF using ASL-MRP. Delayed transit time is a major source of these errors [3, 9, 10]. Effect of delayed transit time can occur even in healthy subjects across the brain. It is stronger in distal branches, especially in regions between perfusion territories known as border-zone areas. In addition, in patients with cerebrovascular disease, this effect can cause major bias in quantitative estimate of cerebral perfusion using ASL-MRP. Consequently, the differentiation between true CBF impairment and delayed transit time based on conventional ASL-MRP has been a challenge. Therefore, even though ASL-MRP has been proven to have potentials to play major roles in many diseases including cerebrovascular diseases, clinical implication of ASL-MRP has been discouraged despite its many advantages.

To overcome this bias caused by delayed transit time, appropriate post-labeling delay (PLD) time for variable patients has been suggested [3, 11]. However, in clinical setting, presumption for the characteristics of patients prior to diagnostic approach including imaging and establishment of appropriate PLD time prior to the acquisition of ASL-MRP are limited. Even though multiple approaches including the look-locker technique and velocity-selective method have been introduced and assessed [12–14], the technical difficulty and limited accessibility of these techniques have rendered their use challenging.

Recently, multi-phase ASL-MRP technique (enhanced ASL technique; General Electric Healthcare, Milwaukee, WI, USA) has been introduced as a method to correct the delayed transit time effect. In this technique, perfusion maps are obtained at seven different PLD times using a modified Hadamard encoding [15, 16]. The Hadamard encoding was modified to acquire an additional reference only image. The multidelay images were used to compute transit time maps and transit time corrected CBF maps [17].

In the present study, we evaluated the usefulness of transit time corrected CBF map based on multi-phase ASL-MRP compared to DSC-MRP.

Methods

Patients

This retrospective study was approved by the Institutional Review Board of Seoul National University Hospital. The requirement for informed consent was waived due to its retrospective nature.

From August 2014 to July 2015, conventional (single-phase), multi-phase ASL-MRPs and DSC-MRP were

acquired for 108 consecutive patients, including those with acute ischemic stroke ($n = 16$), moyamoya disease ($n = 42$), atherosclerosis ($n = 8$), underlying malignancy ($n = 5$), and healthy subjects ($n = 37$). There were 58 men and 50 women patients. The mean age of the 108 patients was 56 years (range, 18–87 years). For male patients, the mean age was 54 years (range, 18–87 years). For female patients, the mean age was 59 years (range, 21–86 years). There was no significant ($P > 0.05$) difference in age between male and female patients. Among these patients, arterial stenosis in the internal carotid artery and/or middle cerebral artery and/or anterior cerebral artery was noted in 34 patients bilaterally and in 27 patients unilaterally.

Perfusion MR imaging

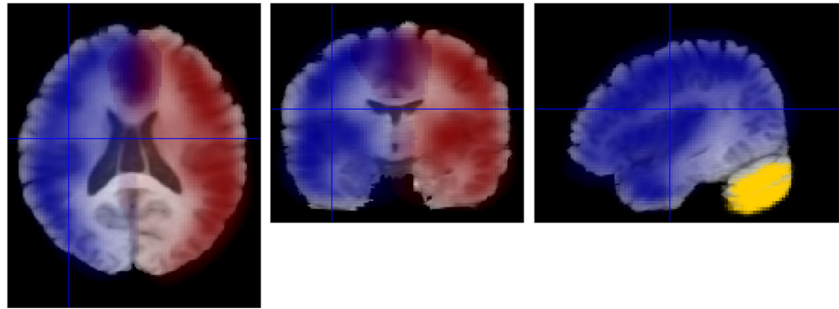
ASL-MRPs and DSC-MRP were acquired sequentially. A 3-T clinical MR imaging unit (Discovery 750 W; General Electric Healthcare, Milwaukee, WI, USA) with a 32-channel head coil was utilized to acquire ASL-MRPs and DSC-MRP. Prior to the acquisition of ASL-MRP and DSC-MRP, axial 3D spoiled gradient-recalled echo (SPGR) T1-weighted images (repetition time = 10.2 ms, echo time = 4.2 ms, flip angle = 12° , field of view = 24×24 cm², slice thickness = 1 mm) were acquired as morphological sequences.

The following multi-phase ASL-MRP protocol was applied to patients: repetition time, 5902 ms; echo time, 11.3 ms; slice thickness, 5 mm; number of averages, 1; number of slices, 28; readout, 4 spiral arms \times 640 samples; field of view, 24×24 cm²; matrix, 128×128 ; and voxel resolution, 3.8 mm \times 3.8 mm \times 5.0 mm. A modified Hadamard encoding technique was used to obtain multi-phase ASL-MRP images in a time and signal-to-noise ratio efficient manner [18]. This sequence produced multi-phase ASL-MRP images at different post label delay times (1.00, 1.22, 1.48, 1.78, 2.15, 2.63, 3.32 s) and effective labeling durations (0.22, 0.26, 0.30, 0.37, 0.48, 0.68, 1.18 s). From this data, a transit time map was computed using the weighted delay method [17] and conventional ASL-MRP (cerebral blood flow without knowledge of the transit time) and transit time corrected ASL-MRP maps were computed [15, 17, 19, 20]. Scan duration was 3 min and 53 s.

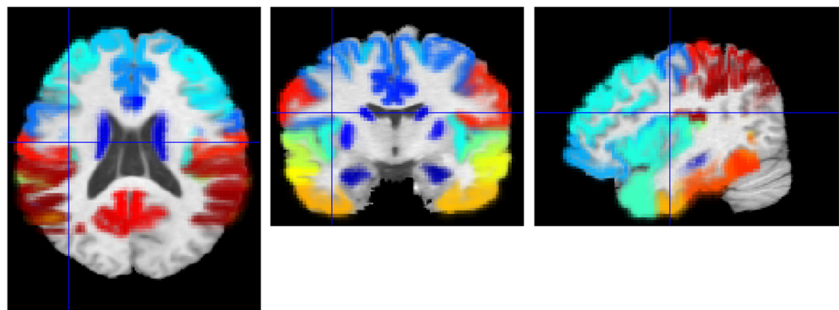
The DSC-MRP parameters applied to patients to obtain axial gradient-recalled-echo images were as follows: repetition time, 1500 ms; echo time, 30 ms; flip angle, 60° ; field of view, 24×24 cm²; matrix, 100×100 ; voxel resolution, 2.4 mm \times 2.4 mm \times 5.0 mm; slice thickness, 5 mm; number of excitations, 1; and number of interleaved slices, 19. For each slice, 60 images were acquired at intervals equal to the repetition time. After approximately eight time points, a standard dose of 0.1 mmol/kg body weight of gadolinium-based contrast agent (Gadovist, Bayer Schering Pharma AG, Berlin,

Fig. 1 Probabilistic vascular territory and anatomical structure-based VOIs. The upper and lower panels show vascular territory-based and anatomical structure-based VOIs. The VOIs for the cerebellum including the bilateral cerebella are also shown in the figure. Partial overlap is noted in the bilateral ICA territories around the midline (upper row)

Vascular territory-based VOIs



Anatomical structure-based VOIs



Germany) was injected intravenously at a rate of 5 mL/s followed by a 20-mL bolus of saline at a rate of 5 mL/s using a power injector (Optistar; Mallinckrodt, St. Louis, MO, USA). Perfusion maps of relative CBF and time to peak (TTP) were generated using commercial software Nordic ICE (NordicNeuroLab, Bergen, Norway). The measured tissue concentration-time curve was deconvolved after eliminating the effect of contrast agent recirculation by using γ -variate fitting [21]. In addition, the arterial input function was identified in the intact middle cerebral artery (MCA) for patients with unilateral occlusion in acute ischemic stroke or unilateral moyamoya disease and in the posterior cerebral artery branch at the level of the basal ganglia for patients with bilateral moyamoya disease. The TTP value was estimated as the interval between the time the contrast agent was administered

and the time it reached its highest concentration in specific areas of interest.

Data preprocessing

All images were preprocessed with SPM5 (Wellcome Department of Cognitive Neurology, University College London, UK) and custom scripts using MATLAB 7.6.0 (R2008a) (The Mathworks Inc., Natick, MA, USA).

Image preprocessing was performed as follows. (a) For DSC-MRPs, CBF and TTP maps of each subject were co-registered to the corresponding 3D SPGR image. First, the initial gradient-echo images were obtained before the injection of contrast agent. These images were obtained precisely using the same positions as the corresponding CBF and TTP maps.

Table 1 General hemodynamic parameters based on DSC-PWI and ASL-PWI

VOIs	nCBF _{DSC}	TTP (s)	nCBF _{Conventional ASL-PWI}	nCBF _{Multi-phase ASL-PWI}
ICA territory-based VOIs (<i>n</i> = 216)	1.11 ± 0.08	8.46 ± 5.63	1.04 ± 0.09	1.04 ± 0.09
Stenotic group (<i>n</i> = 95)	1.12 ± 0.08	9.30 ± 5.78	1.03 ± 0.09	1.04 ± 0.09
Non-stenotic group (<i>n</i> = 121)	1.11 ± 0.06	7.80 ± 5.42	1.05 ± 0.08	1.05 ± 0.08
Anatomical structure-based VOIs (<i>n</i> = 7344)	1.12 ± 0.53	11.76 ± 2.48	1.08 ± 0.38	1.06 ± 0.35
Stenotic group (<i>n</i> = 3230)	1.12 ± 0.53	11.86 ± 2.65	1.07 ± 0.38	1.07 ± 0.36
Non-stenotic group (<i>n</i> = 4114)	1.12 ± 0.53	11.70 ± 2.35	1.08 ± 0.38	1.06 ± 0.35

Data are expressed as mean values ± SD

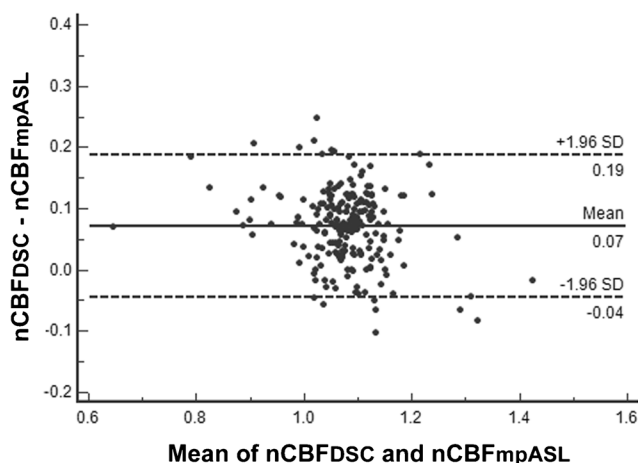
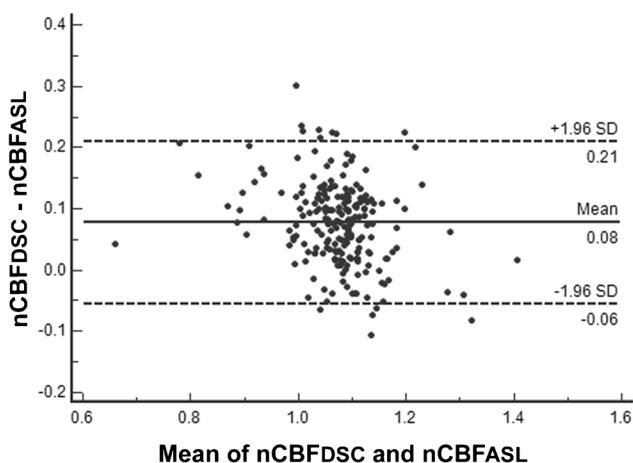
However, they had more anatomical details than CBF maps and TTP maps themselves. The initial gradient-echo images were co-registered to the 3D SPGR T1-weighted images and transformation matrix was obtained. The same transformation matrix was applied for co-registration of CBF and TTP maps. (b) For ASL-MRPs, CBF maps based on conventional ASL-MRP and multi-phase ASL-MRP of each subject were co-registered to the corresponding 3D SPGR image. Initial raw ASL-MRP images before arterial spin labeling taken in exactly the same position as the corresponding CBF maps with more anatomic details than the CBF maps themselves were co-registered to the 3D SPGR T1-weighted images. Transformation matrices were then obtained. The same

transformation matrix was applied to co-register the CBF map. (c) The 3D SPGR T1-weighted images were segmented using prior tissue from ethnicity-specific standard template, a modified version of the Montreal Neurological Institute standard T1 template for the standard Talairach spaces [22]. (d) The 3D SPGR T1-weighted images, CBF and TTP maps from DSC, and CBF maps from ASL-MRP were then spatially normalized using the ethnicity-specific standard template [23].

Definition of volumes of interest

A total of 71 3D volumes of interest (VOIs) were applied to spatially normalized CBF and TTP maps using DSC

Vascular territory-based VOIs



Anatomical structure-based VOIs

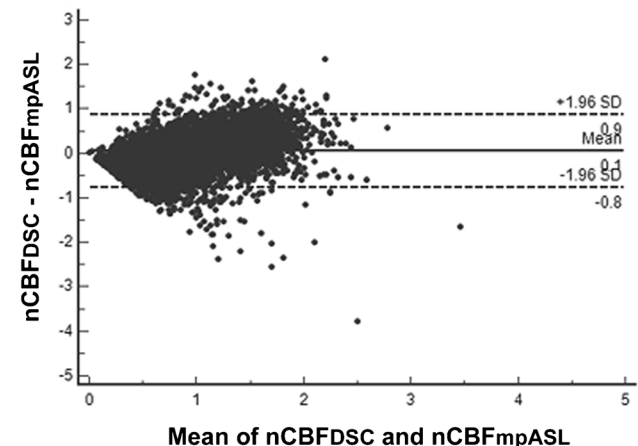
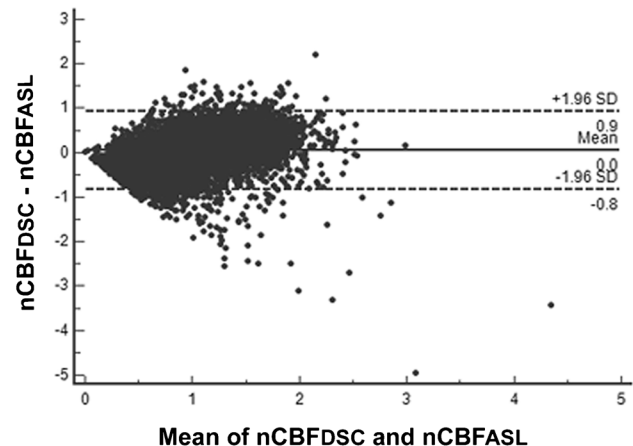


Fig. 2 Concordances between nCBF values obtained from DSC-MRP and ASL-MRP. Bland-Altman plots show the concordances between the nCBF values from DSC-MRO and nCBF values from conventional and multi-phase ASL-MRPs. For the vascular territory-based VOIs, the values of nCBFs from conventional and multi-phase ASL-MRPs had lower values than nCBF based on DSC-MRP (mean differences, 0.08 and 0.07, respectively). The differences between nCBFs from ASL-

MRPs and nCBF from DSC-MRP were similar. For the anatomical structure-based VOIs, the values of nCBFs from conventional and multi-phase ASL-MRPs had similar values with nCBF based on DSC-MRP (mean differences, 0.0 for both). The differences between nCBFs from ASL-MRPs and nCBF from DSC-MRP showed narrower distribution in nCBF from multi-phase ASL-MRP than nCBF from conventional ASL-MRP

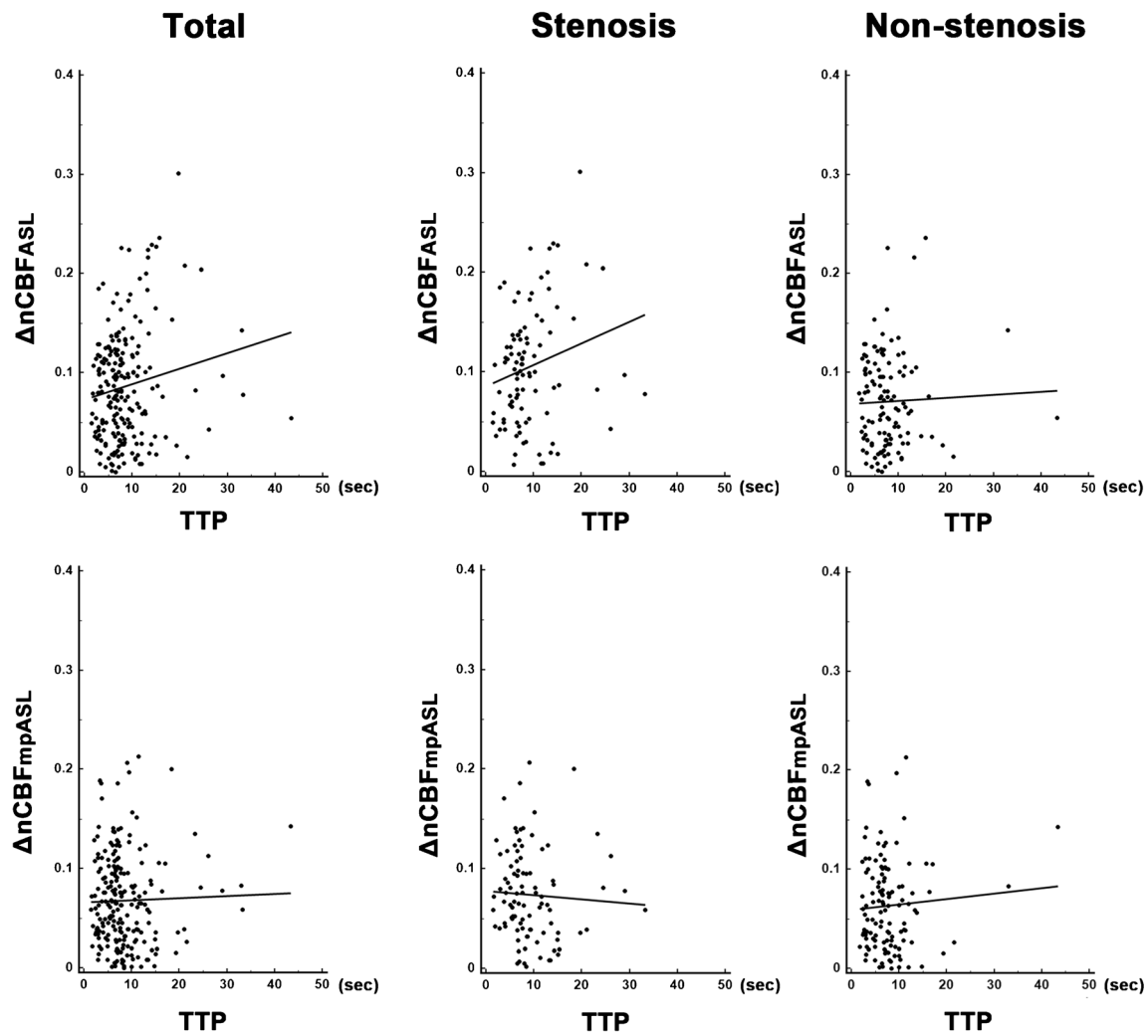


Fig. 3 Regression analysis showing dependence of $\Delta nCBF$ on TTP determined with DSC-MRP from conventional and multi-phase ASL-MRP techniques for vascular territory-based VOIs. These figures show that the dependence of $\Delta nCBF$ on TTP determined with DSC-MRP from conventional ASL-MRP technique can be overcome by applying the

multi-phase ASL-MRP technique for vascular territory-based VOIs. Significant dependence of $\Delta nCBF$ on TTP was revealed only in conventional ASL-MRP for total patients and for those with stenosis. Note: mpASL, multi-phase ASL

and CBF maps from conventional and multi-phase ASL-MRP by a neuroradiologist (TJY with over than 10 years of experience). The VOIs consisted of two vascular territory-based VOIs for internal carotid arteries (ICAs) and 68 anatomical structure-based VOIs within ICA territories. An additional VOI for the cerebellum (including the bilateral cerebellar hemispheres) was used for normalization (Fig. 1). These VOIs were determined according to the previously described perfusion probabilistic map and anatomical probabilistic map. [8, 10, 23–26] Extraction of quantitative CBF value was performed by a neuroradiologist (TJY, with over than 10 years of experience) using SPM5 (Wellcome Department of Cognitive Neurology, University College London, UK) and MarsBaR toolbox of the SPM software package.

Analysis of perfusion MR imaging data

Because CBF values from DSC-MRP have characteristics of relativity, additional adjustment is required to compare CBF values from DSC-MRP and those from ASL-MRP technique. Therefore, normalized CBF value ($nCBF$) was calculated by adjusting CBF values for cerebellar hemispheres as follows:

$$nCBF_{ROI} = CBF_{ROI} / CBF_{cerebellum}$$

In addition, we calculated the difference in normalized CBF values from DSC-MRP and ASL-MRP ($\Delta nCBF$) as follows:

$$\Delta nCBF = nCBF_{DSC-MRP} - nCBF_{ASL-MRP}$$

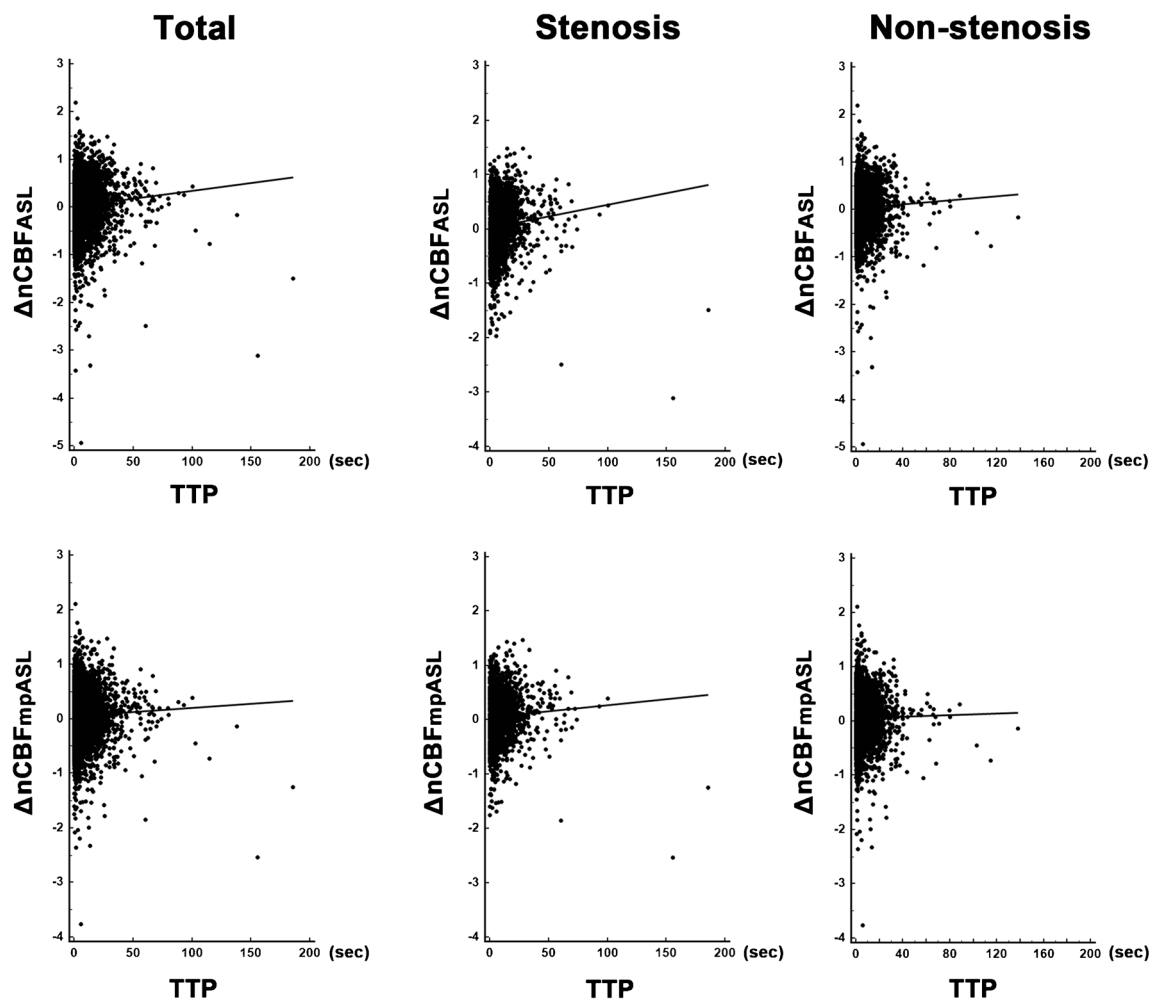


Fig. 4 Regression analysis showing dependence of $\Delta nCBF$ on TTP determined with DSC-MRP from conventional and multi-phase ASL-MRP techniques for anatomical structure-based VOIs. These figures show that the dependence of $\Delta nCBF$ on TTP determined with DSC-MRP from conventional ASL-MRP technique can be overcome after

applying multi-phase ASL-MRP technique for anatomical structure-based VOIs. The significant dependence of $\Delta nCBF$ on TTP determined with DSC was revealed only in conventional ASL-MRP for total patients and for those with stenosis, similar to results for vascular territory-based VOIs (Fig. 3). Note: mpASL, multi-phase ASL

Statistical analysis

The concordances between nCBF from DSC-MRP and nCBFs from conventional and multi-phase ASL-MRPs were evaluated using Bland-Altman analysis. The dependence of $\Delta nCBF$ on TTP obtained from DSC-MRP was analyzed using linear regression analysis. In addition, the same statistical methods were applied for subgroup analysis (stenotic group and non-stenotic group). Statistical analyses were performed using commercially available software ([SPSS, version 12.0 for Windows; SPSS, Chicago, IL, USA] and [MedCalc, version 9.3.0.0; MedCalc Software, Mariakerke, Belgium]). Bonferroni-corrected *P* values of less than 0.05 were considered statistically significant for vascular territory- and anatomical structure-based VOIs.

Results

Mean values and SD values for nCBFs from DSC-MRP and ASL-MRPs are summarized in Table 1.

Analysis of vascular territory-based VOIs

Concordances between nCBF from DSC-MRP and nCBFs from conventional and multi-phase ASL-MRPs

The values of nCBFs from conventional and multi-phase ASL-MRPs had lower values than nCBF based on DSC-MRP (mean differences, 0.08 and 0.07, respectively). The differences between nCBFs from ASL-MRPs and nCBF from DSC-MRP were similar (Fig. 2).

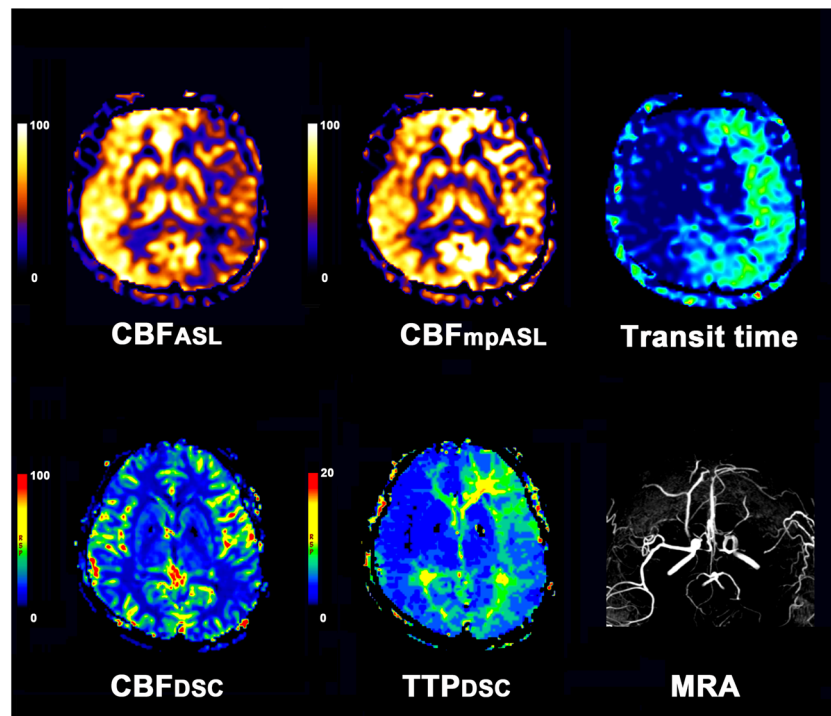


Fig. 5 Representative MR images using conventional and multi-phase ASL-MRP techniques as well as DSC-MRP technique in a patient with moyamoya disease. CBF map based on conventional ASL-MRP technique (left column of the upper row, scale unit of $\text{mL } 100 \text{ g}^{-1} \text{ min}^{-1}$) shows decreased signal intensity in the left MCA territory. CBF map based on multi-phase ASL-MRP technique (middle column of the upper row, scale unit of $\text{mL } 100 \text{ g}^{-1} \text{ min}^{-1}$) shows compensated signal intensity in the left MCA territory. Transit time map based on multi-phase ASL-MRP technique (right column of the upper

row, relative value without scale unit) reveals delayed arterial transit time in the left MCA territory. On the CBF map based on DSC-MRP technique (left column of the lower row, scale unit of $\text{mL } 100 \text{ g}^{-1} \text{ min}^{-1}$), decreased CBF value is not definite in the left MCA territory. However, the delayed transit time can be noted in the left MCA territory on TTP map based on DSC-MRP technique (middle column of the lower row, scale unit of seconds). MRA (right column of the lower row) shows near total occlusion in the left proximal MCA. Note: mpASL, multi-phase ASL

Dependence of ΔnCBF on TTP determined from DSC-MRP

Significant ($F = 5.5679$, $P = 0.0384$) model emerged for vascular territory-based VOIs when conventional ASL-MRP was used. The model is shown below:

$$\Delta\text{nCBF} = 0.073 + 0.001573 \times \text{TTP}$$

However, when multi-phase ASL-MRP was used, significant model failed to emerge ($F = 0.1433$, $P > 0.05$).

For subgroup analysis for VOIs with stenosis ($n = 95$), significant ($F = 4.3331$, $P = 0.0401$) model emerged for vascular territory-based VOIs when conventional ASL-MRP was used. The model is shown below:

$$\Delta\text{nCBF} = 0.085 + 0.002168 \times \text{TTP}$$

However, for multi-phase ASL-MRP, significant model failed to emerge ($F = 0.2694$, $P > 0.05$).

For subgroup analysis of VOIs without stenosis ($n = 121$), significant model did not emerge for vascular territory-based VOIs when conventional or multi-phase ASL-MRP was used ($F = 0.1511$ and 0.5038 , respectively, $P > 0.05$ for both) (Fig. 3).

Analysis of anatomical structure-based VOIs

Concordances between nCBF from DSC-MRP and nCBFs from conventional and multi-phase ASL-MRPs

The values of nCBFs from conventional and multi-phase ASL-MRPs had similar values with nCBF based on DSC-MRP (mean differences, 0.0 for both). The differences between nCBFs from ASL-MRPs and nCBF from DSC-MRP showed narrower distribution in nCBF from multi-phase ASL-MRP than nCBF from conventional ASL-MRP (Fig. 2).

Comparison of correlation coefficients between nCBF values obtained from DSC-MRP and conventional ASL-MRP or multi-phase ASL-MRP

According to Hotelling's t test, significantly greater correlation between nCBF values obtained from DSC-MRP and multi-phase ASL-MRP than that between nCBF values obtained from DSC-MRP and conventional ASL-MRP was found for anatomical structure-based VOIs ($Z = 17.659$, $P < 0.01$).

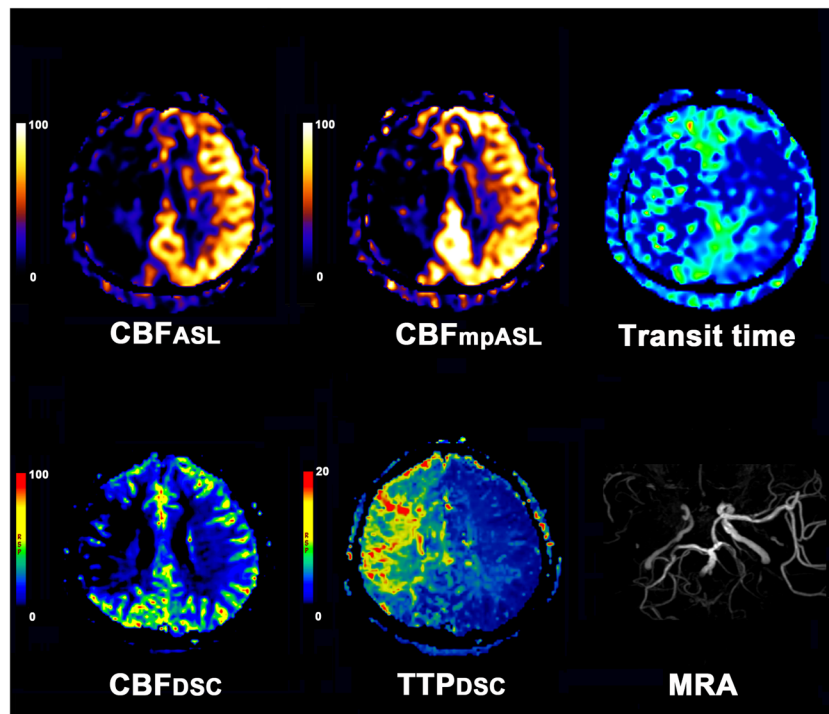


Fig. 6 Representative MR images using conventional and multi-phase ASL-MRP techniques as well as DSC-MRP technique in a patient with atherosclerotic stenosis. CBF map based on conventional ASL-MRP technique (left column of the upper row, scale unit of $\text{mL } 100 \text{ g}^{-1} \text{ min}^{-1}$) shows decreased signal intensity in the right middle cerebral artery (MCA) territory. CBF map based on multi-phase ASL-MRP technique (middle column of the upper row, scale unit of $\text{mL } 100 \text{ g}^{-1} \text{ min}^{-1}$) also shows decreased signal intensity in the right MCA territory. Transit time map based on multi-phase ASL-MRP technique (right column of the upper row, relative value without scale

unit) reveals the delayed arterial transit time in the right MCA territory. On the CBF map based on DSC-MRP technique (left column of the lower row, scale unit of $\text{mL } 100 \text{ g}^{-1} \text{ min}^{-1}$) and TTP map based on DSC-MRP technique (middle column of the lower row, scale unit of seconds), decreased CBF value and delayed transit time are noted in the right MCA territory. MRA (right column of the lower row) shows the near total occlusion in the right proximal MCA. Conventional MR images including T2-weighted image and FLAIR reveal a cerebromalacia with tissue defect, suggesting chronic infarct in the right MCA territory (not shown). Note: mpASL, multi-phase ASL

Dependence of $\Delta n\text{CBF}$ on TTP determined with DSC-MRP

Significant ($F = 23.2302$, $P < 0.0068$) model emerged for anatomical structure-based VOIs when conventional ASL-MRP was used. The model is shown below:

$$\Delta n\text{CBF} = 0.020 + 0.003283 \times \text{TTP}$$

However, when multi-phase ASL-MRP was used, significant model failed to emerge ($F = 7.9309$, $P > 0.05$).

For subgroup analysis of VOIs with stenosis ($n = 3230$), significant ($F = 29.6198$, $P < 0.0068$) model emerged for anatomical structure-based VOIs when conventional ASL-MRP was used. The model is shown below:

$$\Delta n\text{CBF} = 0.022 + 0.002130 \times \text{TTP}$$

However, when multi-phase ASL-MRP was used, significant model failed to emerge ($F = 9.2463$, $P > 0.05$).

In addition, for subgroup analysis of VOIs without stenosis ($n = 4114$), significant model failed to emerge for anatomical structure-based VOIs when conventional or multi-phase ASL-

MRP was used ($F = 6.2539$ and 0.8753 , respectively, $P > 0.05$ for both) (Fig. 4).

Representative images are shown in Figs. 5, 6, and 7.

Discussion

This study demonstrated that the use of transit time corrected CBF maps based on multi-phase ASL-MRP technique could improve the correlation of CBF values between DSC-MRP and ASL-MRP. In addition, this technique could overcome the delayed transit time effect on perfusion maps based on ASL-MRP.

Conventional ASL-MRP usually employs a single PLD typically between 1.5 and 2 s for the quantification of CBF [3, 4, 6, 10, 11]. Therefore, the CBF value based on ASL-MRP will be underestimated in areas in which the arterial transit time is longer than the PLD time. According to previous studies, the effect of delayed transit time is considerable despite of correlations between CBF values from ASL-MRP and DSC-MRP [3, 9, 10]. A previous study has reported that

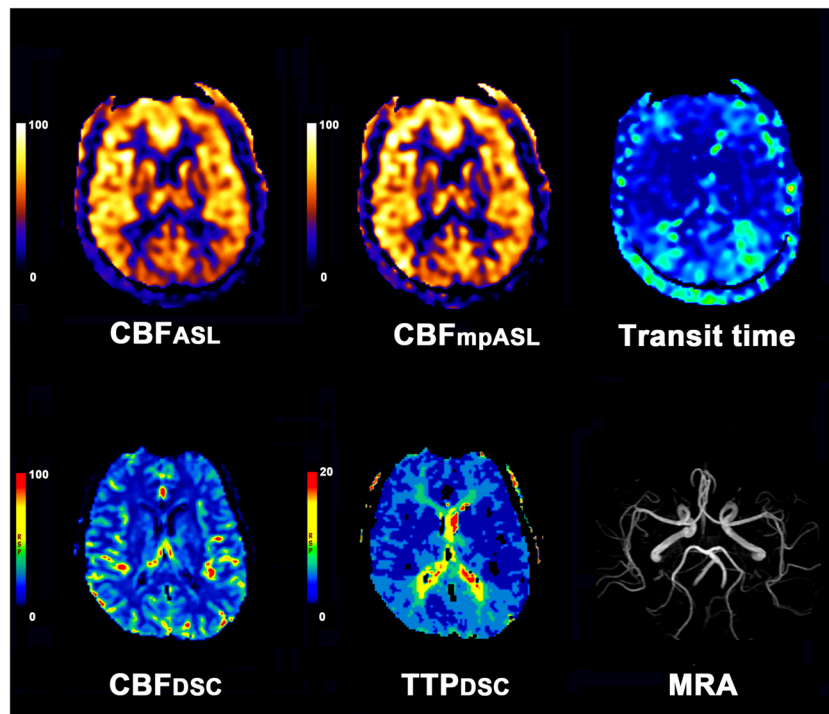


Fig. 7 Representative MR images using conventional and multi-phase ASL-MRP techniques as well as DSC-MRP technique in a healthy subject. CBF map based on conventional ASL-MRP technique (left column of the upper row, scale unit of $\text{mL } 100 \text{ g}^{-1} \text{ min}^{-1}$) shows normal symmetric signal intensities in the bilateral cerebral hemispheres. CBF map based on multi-phase ASL-MRP technique (middle column of the upper row, scale unit of $\text{mL } 100 \text{ g}^{-1} \text{ min}^{-1}$) also shows normal symmetric signal intensities in the bilateral cerebral hemispheres. Transit time map based on multi-phase ASL-MRP

technique (right column of the upper row, relative value without scale unit) reveals no evidence of delayed arterial transit time in the bilateral cerebral hemispheres. On the CBF map based on DSC-MRP technique (left column of the lower row, scale unit of $\text{mL } 100 \text{ g}^{-1} \text{ min}^{-1}$), TTP map based on DSC-MRP technique (middle column of the lower row, scale unit of seconds) shows normal symmetric CBF value without delayed transit time in the brain parenchyma. MRA (right column of the lower row) shows normal intracranial vasculature without stenosis. Note: mpASL, multi-phase ASL

the correlation between CBF values from ASL-MRP and DSC tends to be weaker with increasing TTP [10]. In addition, according to our experience for more than 8 years, the effect of delayed transit time seems to be magnified on ASL-MRP when images are interpreted visually.

Therefore, investigators studying appropriate ASL-MRP techniques have recommended many variable PLD times according to the characteristic of patients [3, 11]. However, in clinical setting, prediction of possible imaging finding that might influence arterial transit time including vascular stenosis is a challenge and subsequent establishment of appropriate PLD time is infeasible. Even though low-resolution prescan of transit delay has been suggested, clinical application of this technique is limited because delayed transit time effect can occur at various degrees even in the same subject. We assume that simultaneous acquisition of information about arterial transit time and transit time corrected CBF map based on information about transit time might be the ideal technique to overcome the delayed transit time effect in conventional ASL-MRP technique.

In the present study, both CBF values from conventional ASL-MRP and transit time corrected CBF map based on multi-phase ASL-MRP technique have high concordance levels with CBF value based on DSC-MRP for both vascular

territory-based VOIs and anatomical structure-based VOIs. In addition, results of regression analysis showed that values of ΔnCBF were dependent on TTP values of conventional ASL-MRP technique for both vascular territory-based VOIs and anatomical structure-based VOIs. There was no dependency of ΔnCBF on TTP values of the multi-phase ASL-MRP technique for vascular territory-based VOIs or anatomical structure-based VOIs. Interestingly, according to subgroup analysis for patients with or without stenosis, the dependency of ΔnCBF on TTP values was found only in subgroup analysis for those with stenosis. It seems that more profound delayed transit time effect in the areas with proximal stenosis contributes the result.

We believe that we can differentiate impaired CBF value and delayed transit time effect using the multi-phase ASL-MRP technique. ASL-MRP images based on integrated images of both conventional and multi-phase ASL-MRP could improve the accuracy in imaging diagnosis. It is feasible to use this imaging analysis based on integrated images to differentiate impaired CBF value and delayed transit time effect (or the combination of impaired CBF value and delayed transit time effect) when we encounter decreased signal intensity on ASL-MRP. However, it should be taken into consideration that transit time

images and conventional ASL-MRP images (also included in ASL images provided in multi-phase MRP techniques as well as transit time corrected ASL images) in which delayed transit time effect is not eliminated can provide clinically relevant information including possible proximal stenosis, presence of occluded vessel, and presence of collateral formation [7, 10, 25, 27].

This study has a few limitations. First, the ICA territory-based VOIs were overlapped around the midline. We used probabilistic ICA territory-based VOIs acquired from perfusion probabilistic maps to evaluate CBF in areas based on blood flow distribution from each large vessel. Overlapping ICA territory-based VOIs around the midline was unavoidable. The partial overlap of ICA territory-based VOIs might have underestimated or overestimated CBF in ipsilateral ICA territories when contralateral ICA was stenotic or intact, respectively. However, we assumed that results from the anatomical structure-based VOIs, in which an overlap did not exist, could compensate for this drawback. Second, for subgroup analysis, we divided VOIs into stenotic and non-stenotic groups according to whether arterial stenosis in the ICA and/or middle cerebral artery and/or anterior cerebral artery existed or not. Therefore, some VOIs for vascular territory or anatomical structure-based VOIs in stenotic subgroup might not have been influenced by stenotic vessels. Finally, to identify the effect of delayed transit time on ASL-MRP, we analyzed DSC-MRP and ASL-MRP due to the lack of hemodynamic parameters representing transit time generalized by the gold standard including PET. An investigation using CBF values obtained using the gold standard technique might be helpful for validating the results of the present study.

The current study demonstrated that transit time corrected CBF maps based on multi-phase ASL-MRP technique could be used to overcome the delayed transit time effect on perfusion maps based on ASL-MRP. The identification of delayed transit time effect on CBF maps based on ASL-MRP could facilitate proper interpretation of ASL-MRP.

Acknowledgements The enhanced ASL-PWI sequence is a work-in-progress prototype (not commercially available) provided by GE.

Compliance with ethical standards

Funding No funding was received for this study.

Conflict of interest The authors declare that they have no conflict of interest.

Ethical approval All procedures performed in the studies involving human participants were in accordance with the ethical standards of the Seoul National University Hospital Institutional Review Board and/or national research committee and with the 1964 Helsinki Declaration and its later amendments or comparable ethical standards. For this type of study formal consent is not required.

Informed consent For this type of retrospective study formal consent is not required.

References

1. Detre JA, Leigh JS, Williams DS, Koretsky AP (1992) Perfusion imaging. *Magn Reson Med* 23(1):37–45. <https://doi.org/10.1002/mrm.1910230106>
2. Detre JA, Rao H, Wang DJ, Chen YF, Wang Z (2012) Applications of arterial spin labeled MRI in the brain. *J Magn Reson Imaging* 35(5):1026–1037. <https://doi.org/10.1002/jmri.23581>
3. Grade M, Hernandez Tamames JA, Pizzini FB, Achten E, Golay X, Smits M (2015) A neuroradiologist's guide to arterial spin labeling MRI in clinical practice. *Neuroradiology* 57(12):1181–1202. <https://doi.org/10.1007/s00234-015-1571-z>
4. Pollock JM, Tan H, Kraft RA, Whitlow CT, Burdette JH, Maldjian JA (2009) Arterial spin-labeled MR perfusion imaging: clinical applications. *Magn Reson Imaging Clin N Am* 17(2):315–338. <https://doi.org/10.1016/j.mric.2009.01.008>
5. Wolf RL, Detre JA (2007) Clinical neuroimaging using arterial spin-labeled perfusion magnetic resonance imaging. *Neurotherapeutics* 4(3):346–359. <https://doi.org/10.1016/j.nurt.2007.04.005>
6. Wong WHE, Maller JJ (2016) Arterial spin labeling techniques 2009–2014. *J Med Imaging Radiat Sci* 47(1):98–107. <https://doi.org/10.1016/j.jmir.2015.08.002>
7. Yoo RE, Yun TJ, Rhim JH, Yoon BW, Kang KM, Choi SH, Kim JH, Kim JE, Kang HS, Sohn CH, Han MH (2015) Bright vessel appearance on arterial spin labeling MRI for localizing arterial occlusion in acute ischemic stroke. *Stroke* 46(2):564–567. <https://doi.org/10.1161/STROKEAHA.114.007797>
8. Yun TJ, Paeng JC, Sohn CH, Kim JE, Kang HS, Yoon BW, Choi SH, Kim JH, Lee HY, Han MH, Zaharchuk G (2016) Monitoring cerebrovascular reactivity through the use of arterial spin labeling in patients with moyamoya disease. *Radiology* 278(1):205–213. <https://doi.org/10.1148/radiol.2015141865>
9. Deibler AR, Pollock JM, Kraft RA, Tan H, Burdette JH, Maldjian JA (2008) Arterial spin-labeling in routine clinical practice, part 1: technique and artifacts. *Am J Neuroradiol* 29(7):1228–1234. <https://doi.org/10.3174/ajnr.a1030>
10. Yun TJ, Sohn CH, Han MH, Kang HS, Kim JE, Yoon BW, Paeng JC, Choi SH, Kim JH, Song IC, Chang KH (2013) Effect of delayed transit time on arterial spin labeling: correlation with dynamic susceptibility contrast perfusion magnetic resonance in moyamoya disease. *Investig Radiol* 48(11):795–802. <https://doi.org/10.1097/RLI.0b013e3182981137>
11. Alsop DC, Detre JA, Golay X, Gunther M, Hendrikse J, Hernandez-Garcia L, Lu H, MacIntosh BJ, Parkes LM, Smits M, van Osch MJ, Wang DJ, Wong EC, Zaharchuk G (2015) Recommended implementation of arterial spin-labeled perfusion MRI for clinical applications: a consensus of the ISMRM perfusion study group and the European consortium for ASL in dementia. *Magn Reson Med* 73(1):102–116. <https://doi.org/10.1002/mrm.25197>
12. Günther M, Bock M, Schad LR (2001) Arterial spin labeling in combination with a look-locker sampling strategy: inflow turbo-sampling EPI-FAIR (ITS-FAIR). *Magn Reson Med* 46(5):974–984. <https://doi.org/10.1002/mrm.1284.abs>
13. Qiu D, Straka M, Zun Z, Bammer R, Moseley ME, Zaharchuk G (2012) CBF measurements using multidelay pseudocontinuous and velocity-selective arterial spin labeling in patients with long arterial transit delays: comparison with xenon CT CBF. *J Magn Reson Imaging* 36(1):110–119. <https://doi.org/10.1002/jmri.23613>
14. Wong EC, Cronin M, W-C W, Inglis B, Frank LR, Liu TT (2006) Velocity-selective arterial spin labeling. *Magn Reson Med* 55(6):1334–1341. <https://doi.org/10.1002/mrm.20906>
15. Dai W, Shankaranarayanan A, Alsop DC (2013) Volumetric measurement of perfusion and arterial transit delay using hadamard

- encoded continuous arterial spin labeling. *Magn Reson Med* 69(4): 1014–1022. <https://doi.org/10.1002/mrm.24335>
16. Gunther M (2007) Highly efficient accelerated acquisition of perfusion inflow series by cycled arterial spin labeling. In: Proceedings of the 15th Annual Meeting of ISMRM, Germany, p 380
 17. Dai W, Robson PM, Shankaranarayanan A, Alsop DC (2012) Reduced resolution transit delay prescan for quantitative continuous arterial spin labeling perfusion imaging. *Magn Reson Med* 67(5):1252–1265. <https://doi.org/10.1002/mrm.23103>
 18. Gunther M (2007) Encoded continuous arterial spin labeling. In: Proceedings of the ISMRM Workshop on Cerebral Perfusion and Brain Function, Brazil
 19. Dai W, Garcia D, de Bazelaire C, Alsop DC (2008) Continuous flow-driven inversion for arterial spin labeling using pulsed radio frequency and gradient fields. *Magn Reson Med* 60(6):1488–1497. <https://doi.org/10.1002/mrm.21790>
 20. Maleki N, Dai W, Alsop DC (2012) Optimization of background suppression for arterial spin labeling perfusion imaging. *MAGMA* 25(2):127–133. <https://doi.org/10.1007/s10334-011-0286-3>
 21. Calamante F, Ganesan V, Kirkham FJ, Jan W, Chong WK, Gadian DG, Connelly A (2001) MR perfusion imaging in moyamoya syndrome: potential implications for clinical evaluation of occlusive cerebrovascular disease. *Stroke* 32(12):2810–2816. <https://doi.org/10.1161/hs1201.099893>
 22. Collins DL, Neelin P, Peters TM, Evans AC (1994) Automatic 3D intersubject registration of MR volumetric data in standardized Talairach space. *J Comput Assist Tomogr* 18(2):192–205. <https://doi.org/10.1097/00004728-199403000-00005>
 23. Lee JS, Lee DS, Kim J, Kim YK, Kang E, Kang H, Kang KW, Lee JM, Kim J-J, Park H-J, Kwon JS, Kim SI, Yoo TW, Chang K-H, Lee MC (2005) Development of Korean standard brain templates. *J Korean Med Sci* 20(3):483–488. <https://doi.org/10.3346/jkms.2005.20.3.483>
 24. Mazziotta J, Toga A, Evans A, Fox P, Lancaster J, Zilles K, Woods R, Paus T, Simpson G, Pike B, Holmes C, Collins L, Thompson P, MacDonald D, Iacoboni M, Schormann T, Amunts K, Palomero-Gallagher N, Geyer S, Parsons L, Narr K, Kabani N, Goualher GL, Boomsma D, Cannon T, Kawashima R, Mazoyer B (2001) A probabilistic atlas and reference system for the human brain: International Consortium for Brain Mapping (ICBM). *Philos Trans R Soc B: Biol Sci* 356(1412):1293–1322. <https://doi.org/10.1098/rstb.2001.0915>
 25. Yun TJ, Sohn C-H, Han MH, Yoon B-W, Kang H-S, Kim JE, Paeng JC, Choi SH, Kim J-H, Chang K-H (2012) Effect of carotid artery stenting on cerebral blood flow: evaluation of hemodynamic changes using arterial spin labeling. *Neuroradiology* 55(3):271–281. <https://doi.org/10.1007/s00234-012-1104-y>
 26. Yun TJ, Cheon J-E, Na DG, Kim WS, Kim I-O, Chang K-H, Yeon KM, Song IC, Wang K-C (2009) Childhood moyamoya disease: quantitative evaluation of perfusion MR imaging—correlation with clinical outcome after revascularization surgery 1. *Radiology* 251(1):216–223. <https://doi.org/10.1148/radiol.2511080654>
 27. Zaharchuk G, Do HM, Marks MP, Rosenberg J, Moseley ME, Steinberg GK (2011) Arterial spin-labeling MRI can identify the presence and intensity of collateral perfusion in patients with moyamoya disease. *Stroke* 42(9):2485–2491. <https://doi.org/10.1161/strokeaha.111.616466>